

Synthesis and Characteristics of Multifunctional Magneto-luminescent Nanoparticles by an Ultrasonic Wave-assisted Stöber Method

Tien Dung Chu^{1*} and Hoang Nam Nguyen^{2,3,4*}

¹Department of Physics, University of Transport and Communications, 3 Cau Giay, Hanoi 10000, Vietnam

²Faculty of Physics, VNU University of Science, 334 Nguyen Trai, Thanh Xuan, Hanoi 10000, Vietnam

³Nano and Energy Center, VNU University of Science, 334 Nguyen Trai, Thanh Xuan, Hanoi 10000, Vietnam

⁴Nanotechnology Program, VNU Vietnam Japan University, Luu Huu Phuoc, My Dinh 1, Nam Tu Liem, Hanoi 10000, Vietnam

*Corresponding authors: chutdung-vly@utc.edu.vn, namnh@hus.edu.vn

Published online: 25 November 2021

To cite this article: Chu, T. D. & Nguyen, H. N. (2021). Synthesis and characteristics of multifunctional magneto-luminescent nanoparticles by an ultrasonic wave-assisted Stöber method. *J. Phys. Sci.*, 32(3), 75–87. <https://doi.org/10.21315/jps2021.32.3.6>

To link to this article: <https://doi.org/10.21315/jps2021.32.3.6>

ABSTRACT: Multifunctional magneto-luminescent nanoparticles (NPs) were synthesised by an ultrasonic wave-assisted Stöber method. The multifunctional NPs are composed of magnetic NPs (Fe_3O_4) and photoluminescent quantum dots (QDs) (ZnS:Mn) in amorphous silica (SiO_2) matrix, which was confirmed by X-ray diffraction, Raman scattering spectroscopy, and transmission electron microscopy (TEM). The multifunctional NPs have high saturation magnetisation at room temperature simultaneously with strong photoluminescence (PL) in visible light, which is promising for biomedical applications.

Keywords: Fe_3O_4 , ZnS:Mn, magneto-luminescent nanoparticles, multifunctional nanoparticles, Stöber method

1. INTRODUCTION

In nanotechnology applications, molecular detections, imaging, diagnostics, and therapeutics of cancer have attracted many considerations. Specifically, semiconductor nanoparticles (NPs) named quantum dots (QDs) have emerged as an efficient replacement for the conventional organic fluorophores in the field

of optical imaging, cell labelling, and diagnostics due to their unique optical advantages of dopant dependent fluorescence emission band with broad excitation, good photostability, high fluorescence intensity, and long fluorescent lifetime.¹⁻⁴ One kind of the QDs, which consists of these all properties, is Mn²⁺ doped ZnS QDs (ZnS:Mn) and has received attention due to its simple fabrication.⁵⁻⁸ Besides, iron oxide in the crystalline form of magnetite, Fe₃O₄, is a widespread material in biomedical applications. The superparamagnetic properties of the Fe₃O₄ NPs can be controlled by applying an external magnetic field, then, the Fe₃O₄ NPs can be used as targeting materials for drug delivery systems, cells separation, etc.⁹⁻¹³

In general, the magnetic NPs containing hydrophobic characteristics are easily aggregated and can be attacked by the immune system and rejected out of the body. In parallel, most of QDs exhibit toxicity to the body.¹⁴⁻¹⁶ To avoid those aggregations and toxicity, these magnetic NPs and QDs are required to be coated with a desirable material that is biocompatible, water-soluble, and nontoxic. Silica with these desirable properties can be considered as a candidate for coating the surfaces of the magnetic NPs and the QDs and has recently received a lot of attention.^{9,10,13,17} Silica shell changes the surface properties of the magnetic NPs from hydrophobic to hydrophilic and screens the magnetic dipolar attractions between magnetic NPs to avoid their aggregation. Moreover, the silica shell with high biocompatibility will decrease the toxicity of the QDs in vivo.¹⁸⁻²⁰ In addition, the existence of a lot of silanol groups in the silica layer can be functionalised with various functional groups on the surface of silica for conjugating with bio-entities, such as aptamer, antibody, etc., which can be used as capture agents of cancer cells.²¹

Recently, the combination of magnetic NPs and QDs, which is called multifunctional magneto-luminescent NPs, has attracted intense attention due to their simultaneous use in applications such as in vivo luminescent imaging and delivery of therapy for cancer treatment.²²⁻²⁴ In the previous paper, we synthesised ZnS:Mn-Fe₃O₄ bifunctional NPs in silica matrix by the inverse microemulsion method.²⁵ In this work, we propose a simple approach to synthesise multifunctional magneto-luminescent NPs in the silica matrix by an ultrasonic wave-assisted Stöber method, which can be easy to produce silica matrix with many solid cores and a porous shell.²⁶⁻²⁸ The structure, morphology, and characteristics of as-prepared samples were investigated. The strong magnetic and high photoluminescent properties of the multifunctional NPs can be used in malignant cell detection, early diagnosis of cancer, and further cancer treatment.

2. EXPERIMENTAL

2.1 Materials

All chemicals were purchased from Sigma-Aldrich (Merck Life Science Vietnam, Ho Chi Minh, Vietnam) and used without further purification. The chemicals were iron(III) chloride hexahydrate (ACS reagent, 97%), iron(II) chloride tetrahydrate (ReagentPlus, 98%), poly(vinylpyrrolidone), ammonia solution (ACS reagent, 28%–30%), ethanol (ACS reagent, 96%), zinc nitrate hexahydrate (reagent grade, 98%), manganese(II) nitrate tetrahydrate (>97%), sodium dodecyl sulphate (ACS reagent, $\geq 99.0\%$), tetraethyl orthosilicate (reagent grade, 98%), and (3-aminopropyl)triethoxysilane. Deionised water was produced from a DI system at the Nano and Energy Center, VNU University of Science (Hanoi, Vietnam).

2.2 Synthesis of Magnetite NPs

The Fe_3O_4 NPs were synthesised by co-precipitation method using $\text{Fe}^{2+}/\text{Fe}^{3+}$ with 1:2 molar ratios from the two chloride salts of FeCl_2 and FeCl_3 .^{25,27} The mixed solution containing 20 ml of 0.5 M FeCl_3 , 20 ml of 0.25 M FeCl_2 , and 100 ml of 0.1 M surfactant polyvinylpyrrolidone (PVP) was vigorously stirred at 800 cycles/min and kept at 70°C before 7 ml of NH_4OH 28% was added to produce the black colour precipitation. The Fe_3O_4 NPs were collected after purifying through a magnetic separation with ethanol several times to decontaminate the residual chemicals. Then, the as-prepared Fe_3O_4 NPs were dispersed in ethanol.

2.3 Synthesis of Mn^{2+} Doped ZnS QDs (ZnS:Mn)

Mn^{2+} doped ZnS NPs were synthesised by an ultrasonic wave-assisted co-precipitation method.^{6,25} For 10% Mn^{2+} doping, 10 ml of 1.0 M zinc nitrate and 10 ml of 0.1 M manganese nitrate were diluted with 100 ml of 0.1 M surfactant sodium dodecyl sulphate ($\text{SDS-CH}_3(\text{CH}_2)_{11}\text{SO}_4\text{Na}$) to obtain the precursor solution. This solution was ultrasonicated with the pulse mode on:off being 2s:1s. The power and frequency of ultrasound were 225 W and 20 kHz, respectively. During the ultrasonication, 11 ml of 1.0 M sodium sulphide solution was slowly dropped into the precursor solution and kept around 10°C. After 2 h, the ZnS:Mn NPs were collected by centrifuging 5 times with deionised water before being dispersed in ethanol.

2.4 Synthesis of Multifunctional Magneto-luminescent NPs (F-Z@SiO₂)

Fifteen ml of the ZnS:Mn 5 mg/ml, 30 ml of the Fe₃O₄ 5 mg/ml, 4.2 ml of the NH₄OH 28%, and 10.5 ml of deionised water were homogeneously dispersed by an ultrasonic bath to get precursor solution. One ml of the tetraethyl orthosilicate (TEOS) and 1.8 ml of the (3-aminopropyl)triethoxysilane (APTES) in 8.2 ml of the ethanol solvent were vigorously stirred for 5 min. Then, this mixed solution was rapidly injected into the precursor solution to start the hydrolysis of the TEOS and APTES with deionised water by ultrasonication for 30 min. Finally, the as-prepared multifunctional magneto-luminescent NPs were rapidly purified by the external strong magnetic field several times with ethanol and deionised water to obtain the pure multifunctional NPs, called F-Z@SiO₂.

2.5 Characterisation

The structure of all the samples was investigated using an X-ray diffractometer (XRD, Bruker D5005) and a Raman scattering spectrometer (Lab RAM HR800, HORIBA) at the VNU University of Science (Hanoi, Vietnam). The morphology of the samples was studied using transmission electron microscopy (TEM) with a JEOL-JEM1010 microscope with an accelerating voltage of 80 kV at the National Institute of Hygiene and Epidemiology (Hanoi, Vietnam). The absorption properties of samples were measured by an ultraviolet-visible absorption spectrometer (UV-Vis, U2450-PC, Shimadzu-Japan) while the photoluminescence (PL) spectra were studied using 325 nm excitation radiation from a He-Cd laser on the Oriel-Spec MS-257 spectrometer at the VNU University of Science. The magnetic properties of samples were investigated on a vibrating sample magnetometer at the VNU University of Science (VSM, digital measurement systems 880, USA).

3. RESULTS AND DISCUSSION

The crystalline structure of all NPs was determined via the XRD spectra as shown in Figure 1. Figures 1(a)–(c) illustrate the XRD spectra of the Fe₃O₄, ZnS:Mn, and F-Z@SiO₂, respectively. The XRD spectrum of the Fe₃O₄ NPs exhibits clear peaks at $2\theta = 30.05^\circ$, 35.49° , 43.41° , 53.53° , 57.34° , and 62.87° corresponding to reflection planes (220), (311), (400), (422), (511), and (440), which were indexed in the inverse spinel structure with Fd-3m space group.^{11,13,28} The lattice parameter of the Fe₃O₄ crystal was calculated as $a = 8.37 \pm 0.03 \text{ \AA}$, in agreement with published results.^{13,28,29} The average crystalline size was calculated as $\bar{D} = 8.9 \pm 2.8 \text{ nm}$ from the Debye Scherrer formula.^{12,13,28}

The as-prepared ZnS:Mn NPs showed diffraction peaks at 29.0° , 48.5° , and 56.8° which could be assigned to (111), (220), and (311) reflection planes. The lattice parameter of the ZnS:Mn NPs obtained from the XRD spectra was $5.34 \pm 0.04 \text{ \AA}$, which revealed that their cubic zinc blende structure of samples was in agreement with the standard spectra on JCPDS 05-0566.⁸ Similar to the Fe_3O_4 NPs, the crystalline diameter of the ZnS:Mn NPs can be estimated as $\bar{D} = 3.3 \pm 0.7 \text{ nm}$. The XRD peaks are broadened due to the nanocrystalline nature of particles. These nanocrystals have lower lattice parameters compared to the bulk, which contributes to the broadening of the peaks in the diffraction spectra. This broadening of the peaks could be caused due to the micro-straining of the defects of the crystal structure such as dislocation and twinning.³⁰ These defects are associated with the chemically synthesised nanocrystals as they grow spontaneously during the chemical reaction. As a result, the chemical ligands get negligible time to diffuse to an energetically favourable site. It could also arise due to a lack of sufficient energy needed by an atom to move to a proper site forming the crystallite.^{3–6}

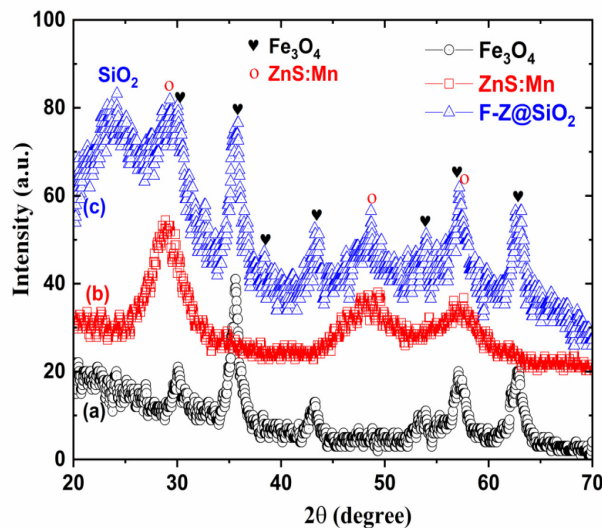


Figure 1: The XRD spectra of all the samples: (a) Fe_3O_4 NPs, (b) ZnS:Mn NPs, and (c) F-Z@ SiO_2 NPs.

The XRD spectra of the multifunctional magneto-luminescent NPs (F-Z@ SiO_2) showed simultaneously all the peaks of Fe_3O_4 and ZnS:Mn nanocrystals in the reflection planes (200), (311), (400), (422), (511), and (440), and (111), (220), and (311), respectively. Moreover, the presence of the new broad peak at 2θ , approximately 22° – 26° , was attributable to the amorphous structure of silica matrix, confirmed the successful coating of the SiO_2 surrounding the Fe_3O_4 NPs and the

ZnS:Mn NPs.^{10,18–20} The XRD spectra of the F-Z@SiO₂ NPs are strong evidence for the encapsulation of the magnetic NPs (Fe₃O₄) and the photoluminescent QDs (ZnS:Mn) in amorphous silica (SiO₂) matrix by an ultrasonic wave assisted Stöber method.^{31,32}

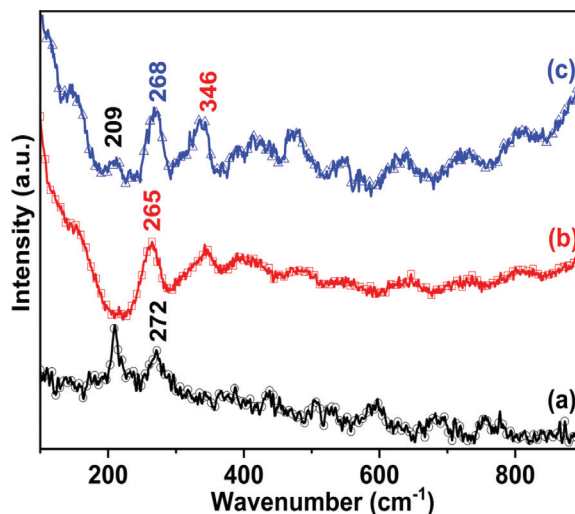


Figure 2: The Raman scattering spectra of all the samples: (a) Fe₃O₄ NPs, (b) ZnS:Mn NPs, and (c) F-Z@SiO₂ NPs.

The Raman scattering spectroscopy is useful to probe the local microstructure. Figures 2(a)–(c) present the Raman scattering spectra of the Fe₃O₄, ZnS:Mn, and F-Z@SiO₂ NPs, respectively. The sharp peaks at 209 cm⁻¹, 272 cm⁻¹, and 605 cm⁻¹ observed in the Fe₃O₄ NPs are a characterisation of the T_{2g}, E_g, and A_{1g} oscillation modes of the Fe₃O₄ nanocrystals.^{13,33} Two wavenumber bands, located surrounding 265 cm⁻¹ and 346 cm⁻¹, were assigned as the characteristic transverse optical (TO) and the longitudinal optical (LO) modes of the cubic zinc blend ZnS:Mn nanocrystals.^{2,5,6} The Raman scattering spectrum of F-Z@SiO₂ showed peaks at 209 cm⁻¹, 268 cm⁻¹, 346 cm⁻¹, and 617 cm⁻¹, that exhibited the T_{2g}, E_g, A_{1g} oscillation modes of the Fe₃O₄ nanocrystals and the TO, LO oscillation modes of the ZnS:Mn nanocrystals simultaneously. Especially, a Raman peak at approximately 268 cm⁻¹, which contained simultaneously the oscillation mode of the ZnS:Mn nanocrystals (at 265 cm⁻¹) and the Fe₃O₄ nanocrystals (at 272 cm⁻¹), was broadened and shifted.⁶ Taken all together, both the XRD and the Raman scattering analyses furnished evidence of the formation of the SiO₂ matrix coating the Fe₃O₄ NPs and ZnS:Mn QDs simultaneously or the pure, highly-crystallised F-Z@SiO₂ multifunctional NPs.

The morphology and size of the as-prepared samples were studied by the TEM as shown in Figure 3. The TEM image of the Fe_3O_4 NPs [Figure 3(a)] displays an almost homogeneous with nearly spherical shape NPs with a diameter of 6–12 nm. This result concurs with the calculated size from the XRD spectra. Besides, the TEM image of the ZnS:Mn NPs [Figure 3(b)] shows that these NPs have a uniform spherical shape and the size ranged from 2.5 nm to 4.5 nm, in agreement with the as-calculated size from the XRD spectra. Figure 3(c) presents the TEM image of the multifunctional magneto-luminescent F-Z@ SiO_2 NPs. In this figure, white circles label ZnS:Mn QDs and red ovals label Fe_3O_4 NPs. This figure also has more fuzzy parts, that are the SiO_2 matrix. The TEM image of the F-Z@ SiO_2 NPs exhibits that the Fe_3O_4 NPs and the ZnS:Mn QDs are encapsulated together in the SiO_2 matrix, which is consistent with the results of the XRD and the Raman scattering.^{31,32}

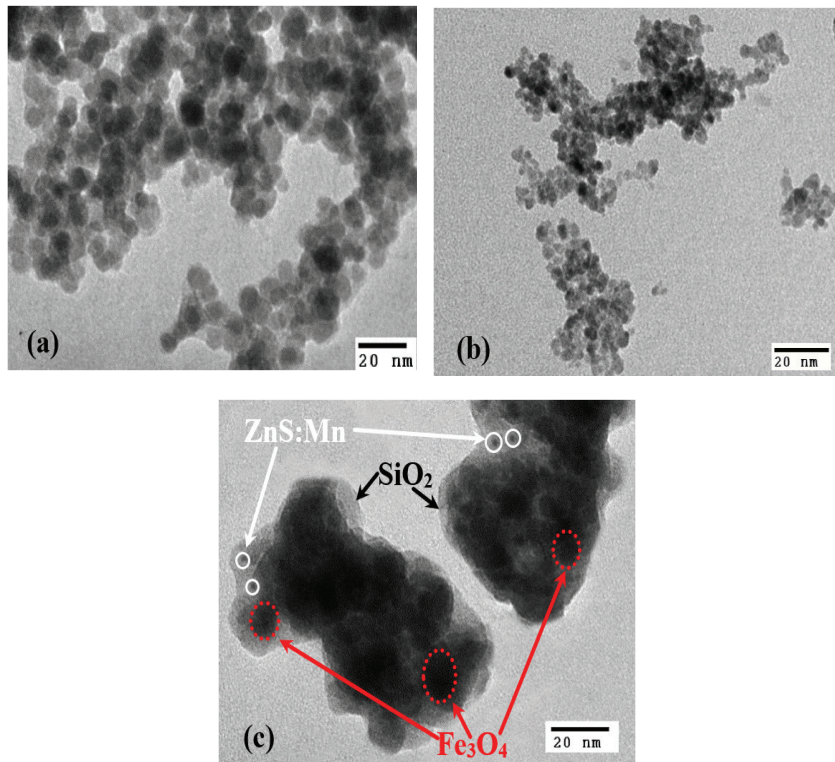


Figure 3: The TEM image of all the samples: (a) Fe_3O_4 NPs, (b) ZnS:Mn NPs, and (c) F-Z@ SiO_2 NPs.

The optical properties of all the samples were studied by the UV-Vis and PL at room temperature, as shown in Figures 4 and 5, respectively. Figure 4 exhibits a sharp absorption edge at 309 nm in the absorption spectra of the ZnS:Mn QDs

and the F-Z@SiO₂ NPs, and no absorption edge in the Fe₃O₄ spectrum. It is well known that the cubic zinc blend ZnS is a direct gap semiconductor. The relation between the absorption coefficients (α) and the incident photon energy ($h\nu$) for the case of allowed direct transition is written as $ah\nu = A(h\nu + E_g)^{1/2}$, where A is a constant and E_g is the bandgap of the material.^{3-8,29} The E_g of the ZnS:Mn QDs and the F-Z@SiO₂ NPs were estimated at approximately 3.76 eV and 3.69 eV, respectively. It was noticed that the E_g values of the ZnS:Mn QDs and the F-Z@SiO₂ NPs were higher than the bandgap value of 3.61 eV at room temperature for the cubic bulk ZnS.⁵⁻⁸ This fact is clear evidence of the quantum confinement effects in the QDs and the multifunctional NPs. The band edge shift towards the lower energy side (redshift) may be due to a partial leakage of the excitons into the surrounding silica matrix.

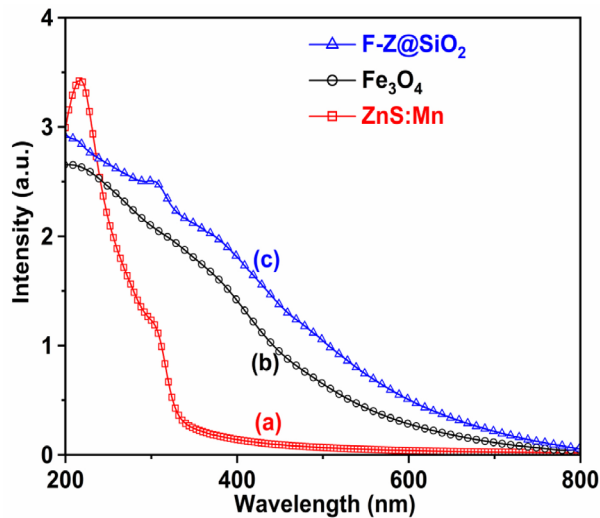


Figure 4: The absorption spectra of (a) ZnS:Mn NPs, (b) Fe₃O₄ NPs, and (c) F-Z@SiO₂ NPs.

Figure 5 shows the PL spectra at room temperature of the ZnS:Mn QDs and the F-Z@SiO₂ NPs, excited at the wavelength of 325 nm. The PL spectra clearly show two major photoluminescent bands. One broad blue-green emission peak, placed at about 2.76 eV (449 nm), arose due to the cubic zinc blend phase. In detail, multi-peaks were fitted by the Gaussian functions such as dash-dot lines in Figure 5. The fitting peaks, centred at 2.97 eV (417 nm), 2.76 eV (449 nm), 2.59 eV (479 nm), and 2.46 eV (504 nm), arose due to the interstitial sulphur (I_S) lattice defects, the interstitial zinc (I_{Zn}) lattice defects, the sulphur vacancies (V_S), and the zinc vacancies (V_{Zn}), respectively.⁶⁻⁸ Another orange peak, located at about 2.07 eV (598 nm), was assigned to the ${}^4T_1 - {}^6A_1$ transition within the 3d shell of

Mn²⁺ doped. The intensity of the orange peak is higher than that of the former peak. The presence of the orange emission indicates that Mn²⁺ has been successfully incorporated into the crystalline lattice of ZnS NPs.^{5–8} However, the intensity of the orange emission of the F-Z@SiO₂ NPs is lower than that of the ZnS:Mn NPs, which is in agreement with the results of the absorption edge. This can be explained as due to the silica matrix coating all the ZnS:Mn NPs and the Fe₃O₄ NPs simultaneously. The high orange emission peak of multifunctional NPs can be used for labelling cells and taking photoluminescent imaging in biomedicine.^{1–8,21} This can be visually expressed, as shown in the inset PL image of the Fe₃O₄ NPs and the F-Z@SiO₂ NPs solution (Figure 5), using the excitation laser beam with the wavelength of 325 nm.

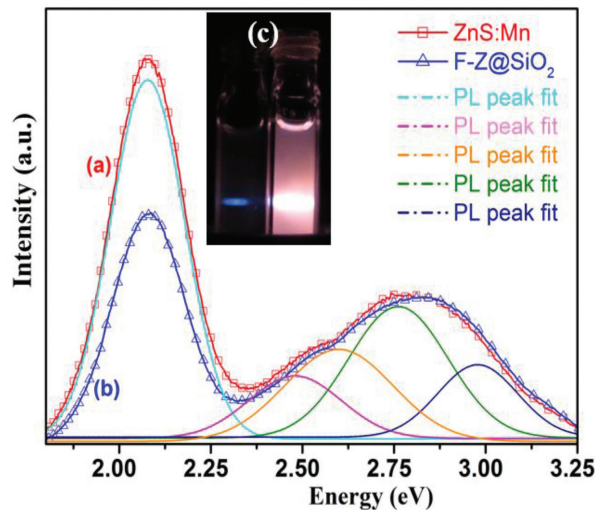


Figure 5: The PL of (a) ZnS:Mn NPs, (b) F-Z@SiO₂ NPs, and (c) inset PL image (excited wavelength is 325 nm).

As can be seen in Figure 6, the magnetic hysteresis loops indicate that the Fe₃O₄ NPs and the F-Z@SiO₂ NPs are superparamagnetic at room temperature with high saturation magnetisation (M_s) (about 61.7 emu/g and 39.5 emu/g for Fe₃O₄ NPs and the F-Z@SiO₂ NPs at 10.5 kOe, respectively) with almost zero coercivity (H_c) and zero remanences (M_r).^{13,19,20} The high M_s of the F-Z@SiO₂ NPs can be attracted more rapidly under an external magnetic field.^{29,31,32} Meanwhile, the magnetisation curve of the ZnS:Mn NPs shows that their magnetisation is very low.^{5,6} Moreover, the decrease of the measured M_s values of the F-Z@SiO₂ NPs can be explained by the formation of the amorphous silica matrix (non-magnetics), covering the Fe₃O₄ NPs and the ZnS:Mn NPs (very low magnetism) simultaneously.²⁸ These results are inconsistent with the results of the XRD, Raman scattering, TEM, and

PL. These magnetic properties are promising to apply for cell separation, drug delivery, as well as MRI.^{9-13,18-20}

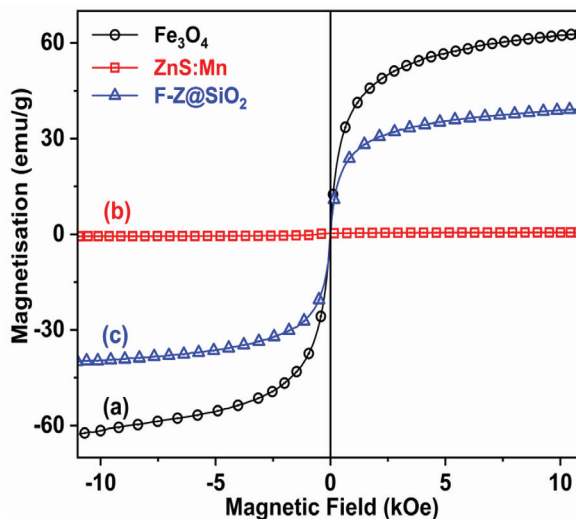


Figure 6: The magnetic hysteresis loops of (a) Fe₃O₄ NPs, (b) ZnS:Mn NPs, and (c) F-Z@SiO₂ NPs.

4. CONCLUSION

The multifunctional magneto-luminescent NPs were successfully synthesised by an ultrasonic wave-assisted Stöber method. The multifunctional F-Z@SiO₂ NPs simultaneously contain magnetite NPs and Mn²⁺ doped ZnS QDs in biocompatible amorphous SiO₂ matrix, which can be further functionalised with various functional groups for conjugating with bioentities, such as aptamer, antibody, etc., to apply in biomedical applications. The multifunctional NPs are superparamagnetic with high saturation magnetisation at room temperature and have strong PL in visible light (598 nm). Then, they can be applicable for malignant cell detection-separation, early diagnosis of cancer, as well as for further cancer treatment.

5. ACKNOWLEDGEMENTS

This study was supported by the Ministry of Science and Technology, Vietnam under Grant DTDL.CN-02/18. This work was also supported by the Ministry of Education and Training, Vietnam, under Grant No. B2020-GHA-04.

6. REFERENCES

1. Byers, R. J. & Hitchman, E. R. (2011). Quantum dots brighten biological imaging. *Prog. Histochem. Cytochem.*, 45(4), 201–237. <https://doi.org/10.1016/j.proghi.2010.11.001>
2. Biju, V. et al. (2010). Bioconjugated quantum dots for cancer research: Present status, prospects and remaining issues. *Biotechnol. Adv.*, 28(2), 199–213. <https://doi.org/10.1016/j.biotechadv.2009.11.007>
3. Hild, W. A., Breunig M. & Goepferich A. (2008). Quantum dots – Nano-sized probes for the exploration of cellular and intracellular targeting. *Eur. J. Pharm. Biopharm.*, 68(2), 153–168. <https://doi.org/10.1016/j.ejpb.2007.06.009>
4. Gao, X. et al. (2004). In vivo cancer targeting and imaging with semiconductor quantum dots. *Nat. Biotechnol.*, 22(8), 969–976. <https://doi.org/10.1038/nbt994>
5. Bui, H. V. et al. (2014). Optical and magnetic properties of Mn-doped ZnS nanoparticles synthesized by a hydrothermal method. *IEEE Trans. Magn.*, 50(6), 1–4. <https://doi.org/10.1109/TMAG.2014.2300187>
6. Kripal, R. et al. (2010). Photoluminescence and photoconductivity of ZnS:Mn²⁺ nanoparticles synthesized via co-precipitation method. *Spectrochim. Acta A Mol. Biomol. Spectrosc.*, 76(5), 523–530. <https://doi.org/10.1016/j.saa.2010.04.018>
7. Yu, J. H. et al. (2013). High-resolution three-photon biomedical imaging using doped ZnS nanocrystals. *Nat. Mater.*, 12, 359–366. <https://doi.org/10.1038/nmat3565>
8. Heo, J. & Hwang, C. S. (2015). Surface properties and photocatalytic activities of the colloidal ZnS:Mn nanocrystals prepared at various pH conditions. *Nanomaterials*, 5(4), 1955–1970. <https://doi.org/10.3390/nano5041955>
9. Quy, D. V. et al. (2013). Synthesis of silica-coated magnetic nanoparticles and application in the detection of pathogenic viruses. *J. Nanomater.*, 603940. <https://doi.org/10.1155/2013/603940>
10. Pham, Y. et al. (2015). Specificity and processing rate enhancement of mycobacterium tuberculosis diagnostic procedure using antibody-coupled magnetic nanoparticles. *Int. J. of Nanotech.*, 12(5/6/7), 335–346. <https://doi.org/10.1504/IJNT.2015.067892>
11. Sun, C., Sze, R. & Zhang, M. (2006). Folic acid-PEG conjugated superparamagnetic nanoparticles for targeted cellular uptake and detection by MRI. *J. Biomed. Mater. Res. A.*, 78(3), 550–557. <https://doi.org/10.1002/jbm.a.30781>
12. Zhang, X. et al. (2016). Iron oxide nanoparticles induce autophagosome accumulation through multiple mechanism: Lysosome impairment, mitochondrial damage and ER stress. *Mol. Pharm.*, 13(7), 2578–2587. <https://doi.org/10.1021/acs.molpharmaceut.6b00405>
13. Xie, Y. et al. (2016). Size-dependent cytotoxicity of Fe₃O₄ nanoparticles induced by biphasic regulation of oxidative stress in different human hepatoma cells. *Int. J. Nanomed.*, 11, 3557–3570. <https://doi.org/10.2147/IJN.S105575>
14. Chou, L. Y. T. & Chan, W. C. W. (2012). No signs of illness. *Nat. Nanotechnol.*, 7, 416–417. <https://doi.org/10.1038/nnano.2012.110>

15. Wegner, K. D. & Hildebrandt, N. (2015). Quantum dots: Bright and versatile in vitro and in vivo fluorescence imaging biosensors. *Chem. Soc. Rev.*, 44(14), 4792–4834. <https://doi.org/10.1039/C4CS00532E>
16. Hauck, T. S. et al. (2010). In vivo quantum-dot toxicity assessment. *Small*, 6(1), 138–144. <https://doi.org/10.1002/sml.200900626>
17. Narita, A., Naka, K. & Chujo, Y. (2009). Facile control of silica shell layer thickness on hydrophilic iron oxide nanoparticles via reverse micelle method. *Colloids Surf. A Physicochem. Eng. Asp.*, 336(1–3), 46–56. <https://doi.org/10.1016/j.colsurfa.2008.11.013>
18. Mahdavi, M. et al. (2013). Fabrication and characterization of SiO₂/(3-Aminopropyl) triethoxysilane-coated magnetite nanoparticles for lead(ii) removal from aqueous solution. *J. Inorg. Organomet. Polym.*, 23, 599–607. <https://doi.org/10.1007/s10904-013-9820-2>
19. Li, Y. S. et al. (2010). Preparation and characterization of silica coated iron oxide magnetic nanoparticles. *Spectrochim. Acta A Mol. Biomol. Spectrosc.*, 76(5), 484–489. <https://doi.org/10.1016/j.saa.2010.04.004>
20. Zhan, S. et al. (2014). Efficient removal of pathogenic bacteria and viruses by multifunctional amine-modified magnetic nanoparticles. *J. Hazard. Mater.*, 274, 115–123. <https://doi.org/10.1016/j.jhazmat.2014.03.067>
21. Hu, Z. et al. (2017). Aptamer combined with fluorescent silica nanoparticles for detection of hepatoma cells. *Nanoscale Res Lett.*, 12(1), 96–103. <https://doi.org/10.1186/s11671-017-1890-6>
22. Beltran-Huarac, J. et al. (2016). Novel magneto-luminescent effect in LSMO/ZnS:Mn nanocomposites at near-room temperature. *Nanotechnology*, 27(8), 085703. <https://doi.org/10.1088/0957-4484/27/8/085703>
23. Koole, R. et al. (2009). Magnetic quantum dots for multimodal imaging. *Wiley Interdiscip. Rev. Nanomed. Nanobiotechnol.*, 1(5), 475–491. <https://doi.org/10.1002/wnan.14>
24. Mahajan, K. D. et al. (2013). Magnetic quantum dots in biotechnology – Synthesis and applications. *Biotechnol. J.*, 8(12), 1424–1434. <https://doi.org/10.1002/biot.201300038>
25. Dung, C. T. et al. (2016). Synthesis of ZnS:Mn-Fe₃O₄ bifunctional nanoparticles by inverse microemulsion method. *J. Sci. Adv. Mater. Dev.*, 1(2), 200–203. <https://doi.org/10.1016/j.jsamd.2016.06.006>
26. Stöber, W., Fink, A. & Bohn, E. (1968). Controlled growth of monodisperse silica spheres in the micron size range. *J. Colloid Interface Sci.*, 26(1), 62–69. [https://doi.org/10.1016/0021-9797\(68\)90272-5](https://doi.org/10.1016/0021-9797(68)90272-5)
27. Keane, D. A. et al. (2010). A modified Stöber process for the production of mesoporous Sub 2 micron silica microspheres; applications in HPLC. *J. Porous Mater.*, 17, 145–152. <https://doi.org/10.1007/s10934-009-9274-7>
28. Dung, T. C. et al. (2017). Synthesis of bifunctional Fe₃O₄@SiO₂-Ag magnetic-plasmonic nanoparticles by an ultrasound assisted chemical method. *J. Electron. Mater.*, 46(6), 3646–3653. <https://doi.org/10.1007/s11664-017-5421-0>

29. Chu, T. D. et al. (2020). Synthesis and properties of magnetic - Semiconductor $\text{Fe}_3\text{O}_4/\text{TiO}_2$ heterostructure nanocomposites for applications in wastewater treatment. *J. Magn.*, 25(1), 1–7. <https://doi.org/10.4283/JMAG.2020.25.1.001>
30. Firdous, A., Singh, D. & Ahmad, M. M. (2013). Electrical and optical studies of pure and Ni-doped CdS quantum dots. *Appl. Nanosci.*, 3, 13–18. <https://doi.org/10.1007/s13204-012-0065-0>
31. Sun., L. et al. (2010). Synthesis of magnetic and fluorescent multifunctional hollow silica nanocomposites for live cell imaging. *J. Colloid Interface Sci.*, 350(1), 90–98. <https://doi.org/10.1016/j.jcis.2010.06.041>
32. Ren, C. et al. (2008). Synthesis of organic dye-impregnated silica shell-coated iron oxide nanoparticles by a new method. *Nanoscale Res. Lett.*, 3, 496–501. <https://doi.org/10.1007/s11671-008-9186-5>
33. Shebanova, O. N. & Lazor, P. (2003). Raman spectroscopic study of magnetite (FeFe_2O_4): A new assignment for the vibrational spectrum. *J. Solid State Chem.*, 174(2), 424–430. [https://doi.org/10.1016/S0022-4596\(03\)00294-9](https://doi.org/10.1016/S0022-4596(03)00294-9)